RESEARCH ARTICLE





Development of branched polyphenolic poly(beta amino esters) to facilitate post-synthesis processing

Kelley Wiegman¹ | Nicolas J. Briot¹ | J. Zach Hilt¹ | Aron J. Huckaba² | Thomas D. Dziubla¹

Correspondence

Thomas D. Dziubla, Department of Chemical and Materials Engineering, 177 F. Paul Anderson Tower, University of Kentucky, Lexington, KY 40506, USA.
Email: thomas.dziubla@uky.edu

Funding information

NIH SBIR, Grant/Award Number: R44DE023523; National Science Foundation, Grant/Award Numbers: ECCS-1542164, 1849213; Kentucky State Matching Grant

Abstract

Given their versatility and formability, polymers have proven to be a viable platform facilitating a controlled and tuned release for a variety of therapeutic agents. One growing area of polymer drug delivery is polymeric prodrugs, which covalently link active pharmaceutical ingredients to a polymeric form to enhance stability, delivery, and pharmacology. One such class of polymeric prodrugs, poly(beta amino esters) (PBAEs) can be synthesized into crosslinked, or "thermoset," networks which greatly limits their processability. An antioxidant-PβAE polymer prodrug that is soluble in organic solutions would permit enhanced processability, increasing their utility and manufacturability. Curcumin PβAEs were synthesized to be soluble in organic solvents while retaining the release and activity properties. To demonstrate the polymer processability, curcumin PβAEs were further synthesized into nanoparticles and thin films. Control over nanoparticle size and film thickness was established through variance of dope solution concentration and withdrawal speed, respectively. Layering of polymeric films was demonstrated through inkjet printing of thin films. Polymer function was characterized through curcumin release and antioxidant activity. The processing of the polymer had a drastic impact on the curcumin release profiles indicating the polymer degradation was influenced by surface area and porosity of the final product. Previously, release was controlled primarily through the hydrophobicity of the polymer. Here, we demonstrate a novel method for further tuning the degradation by processing the polymer.

KEYWORDS

antioxidant, controlled release, poly(beta amino ester) (PβAE)

1 | INTRODUCTION

J Biomed Mater Res. 2022;1-13.

Polymers have been instrumental in the design and formulation of numerous pharmaceuticals, owing to their ability to control the release of the active pharmaceutical ingredients (API). Polymers can be designed to exhibit controlled and targeted release, be stimuli-responsive, and have the ability to tune mechanical properties to facilitate delivery of vastly different APIs for specific clinical needs. ^{1–5} Traditional polymer forms have been very successful at stabilizing drugs

from crystallization enhancing the bioavailability in the process and allowing for a tailored release to specific sites. However, some APIs have proven to be especially challenging to formulate, especially in novel implantable and injectable forms. For instance, when integrating monomers with instability, solubility, or mechanical limitations, these properties can often be passed on to the polymeric form of the API. Certain polymers can integrate additional functional groups or comonomers to help counteract these shortcomings, but care needs to be taken to ensure the degradation products of the polymer do not

¹Department of Chemical and Materials Engineering, University of Kentucky, Lexington, Kentucky, USA

²Department of Chemistry, University of Kentucky, Lexington, Kentucky, USA

introduce a source of toxicity. For successful polymeric delivery of APIs, the API needs to be delivered per the desired release without causing negative side effects.

An example of an active ingredient with solubility and stability limitations are polyphenols. Polyphenols are a class of compounds characterized by the presence of one or more benzene rings with hydroxyl functionalities and are reported to have poor bioavailability due in part to poor thermal and oxidative stability, poor absorption, and low water solubility. However, these compounds have been the subject of intense interest due to potential health benefits such as having anti-inflammatory, antioxidant, anti-inflammatory, antioxidant, and cardioprotective, antimicrobial, and cardioprotective effects. In order to properly utilize these compounds, it is important to retain their native activity upon delivery. This can be achieved through polymeric prodrug synthesis as it allows for increased stability and prevention of premature oxidation compared to free polyphenolic delivery.

Previously, our group has demonstrated the ability to incorporate polyphenols into poly(beta amino ester), or PBAE, based polymers taking advantage of their biodegradability, responsiveness, and compatibility. 16 These polymers are synthesized through the Michael addition of an acrylate and amine and often take on properties similar to their monomers. Due to the structural diversity of PBAEs and the wide array of monomers, it facilitates the ability to fabricate numerous formulations to fulfill various requirements for drug delivery. For instance, drugs can be synthesized into the backbone of the PβAE, thus allowing for increased solubility and circulation in the body with effective accumulation at the targeted site. 17 Similarly, polyphenols can be seamlessly integrated into the PBAE backbone helping to increase the half-life of the polyphenol. Incorporation of the polyphenols into the backbone is feasible through acrylation of the hydroxyl groups for further reaction with an amine group. 18 Due to the wide array of polyphenolic benefits, the incorporation of these molecules into a PBAE delivery system further enhances the versatility and potential applications of these polymers.

Due to the amount of research on PβAEs, much has been learned about how to control degradation rates, extent of reactions, and various mechanical properties of the final polymer. For example, previous work in our lab has been done to demonstrate the controlled, tunable release of curcumin using crosslinked PβAEs. 11,15,19-21 Curcumin is a polyphenol possessing antioxidant properties²²⁻²⁴ and through PβAE delivery, it was demonstrated to retain its antioxidant properties and be utilized for combating oxidative stress. 15,20-26 Much of this work centered on synthesizing crosslinked PBAEs for polyphenolic delivery, but these networks limited the processability of the polymer. These thermoset PBAE systems have been cryomilled down into microparticles for modulating oxidative stress¹⁹ and synthesized into nanogels to facilitate delivery to mitochondria. 11,27 While these techniques help to enable certain routes of delivery, other applications such as the development of homogenous creams, coatings, and castings become difficult with this crosslinked system.

A P β AE polymer that is soluble in organic solvents greatly increases the processing methods options available for their use. Polymer solubility has a large impact on the properties of the

thermodynamically stable polymer solution. This solution is referred to as a dope solution and is required for techniques such as polymer coatings, solvent castings, nanoparticle synthesis, dry/wet spinning, etc. Soluble polymers are often linear or branched in structure as networked systems tend to swell in organic solvents. A promising application of linear PBAEs is in nonviral gene delivery due to its biodegradability. The polymers can combine and condense with the DNA to form complexes allowing for cellular uptake and successful gene transfection. 28-32 Current applications of branched PBAE polymers are also focused on gene delivery and enhancing transfection efficacy over linear PβAE polymer/DNA complexes.^{33–35} In principle, the synthesis of branched PβAE polymers could also create an opportunity for performing hot melt extrusions, injection moldings, etc. permitted the active pharmaceutical ingredient can withstand the processing temperatures. Due to the enhanced solubility of the polymer, the increased processing ability allows for increased delivery options such as nanoparticles, stent coatings, bolus extrudates, solvent castings of thin films, 3-D printed tablets, etc. Many of these processing methods are already developed, making it an easier transition and scale-up to an industrial setting.

This work focuses on introducing an organic soluble polyphenolic PBAE with the intention for the improvement and expansion of delivery methods. While much of the foundation has been paved for increasing the understanding about the control over polyphenolic PβAE delivery, little has been done to improve the method of delivery. The introduction of polyphenols into soluble PBAE polymers could facilitate the potential development of tablets, coatings, and nanoparticles among other methods. With previous polyphenolic PβAEs, little processing has been performed on the polymers to analyze how delivery could be enhanced or made easier in part due to their limited solubility. The antioxidant curcumin was incorporated into the backbone of a branched PBAE structure to demonstrate a controlled and enhanced delivery as compared to free molecule delivery. Due to the branched, but not fully crosslinked, polymeric structure, it was soluble in an organic solvent and could then be processed into nanoparticles and thin coatings to explore alternate delivery methods. The degradation rate and antioxidant activity of each delivery method was determined to demonstrate a controlled release of the active ingredient curcumin and a retention of its antioxidant activity. By increasing the polymer solubility, it allowed for the opportunity to develop novel polyphenolic PBAE delivery methods without sacrificing the control over delivery or the polyphenol's native activity.

2 | MATERIALS AND METHODS

2.1 | Materials

Curcumin used for the curcumin multiacrylate (CMA) was purchased from Chem-Impex International Inc. Acryloyl chloride, anhydrous magnesium sulfate, potassium carbonate, Tween 80, isobutylamine, 2,2'-azino-bis(3-ethylbenzothizoline-6-sulphonic acid) (ABTS), Trolox, and ammonium persulfate (APS) were all purchased from Sigma Aldrich. Triethylamine and

sodium phosphate dibasic dodecahydrate were purchased from Acros Organics. Hydrochloric acid, sodium hydroxide, acetic acid, o-phosphoric acid, and citric acid monohydrate were purchased from Fisher Scientific. Potassium chloride was purchased from BDH chemicals. Poly(ethylene glycol) 400 diacryate (PEG400DA) was purchased from Polysciences. All organic solvents were purchased from Pharmco-AAPER.

2.2 | Synthesis and characterization of the P β AE polymer

To synthesize the soluble PβAE bulk polymer for this study, functionalized curcumin monomer was reacted with the primary amine, isobutylamine (IBA), in anhydrous DCM through Michael addition chemistry. The hydroxyl groups on curcumin were functionalized to acrylate groups as previously demonstrated by our lab group to create the monomer, curcumin multiacrylate or CMA. 18 The product was confirmed through comparison to literature utilizing high performance liquid chromatography (HPLC; Waters Phenomenex C18 column, 5 μ m, 250 mm (length) \times 4.6 mm (I.D.) on a Shimadzu Prominence LC-20 AB Workstation). 18 The column was maintained at 40°C and a gradient of 60/40 acetonitrile/0.1 M o-phosphoric acid to 100/0 acetonitrile/0.1 M o-phosphoric acid over 20 minutes with a 1 ml/min flow rate was utilized. For polymer synthesis, the amount of anhydrous DCM utilized was 1.5 times the total monomer weight. The ratio of CMA to PEG400DA was varied (90:10, 80:20, 70:30, 60:40, and 50:50) and the ratio of total acrylates to amine protons was 0.8 to limit polymer conversion. The first step was to solubilize the CMA in anhydrous DCM (volume of 0.75 times the total monomer weight). The remaining anhydrous DCM was mixed with PEG400DA, IBA was added to the PEG400DA and allowed to react for 5 min at room temperature due to the reactivity of the acrylate components. The CMA mixture was then added to the reaction while being vortexed. The final mixture was poured into an aluminum tin, covered with a watch glass, and allowed to set for 3 h at room temperature. Afterward, it was placed in a convection oven for 24 h at 50°C still covered by the watch glass. The polymer was then washed to remove unreacted monomer and acrylates. The polymer was dissolved in anhydrous DCM and precipitated out using cold diethyl ether in a 1:10 DCM to diethyl ether ratio. The supernatant was then removed, and the polymer dried through rotary evaporation. Gel permeation chromatography (GPC) was performed on a Shimadzu Prominence LC-20 AB Workstation with a Waters 2410 Refractive Index Detector using an Agilent Resipore 300×7.5 mm column. The column was maintained at 40°C and an isocratic flow of 100/0 tetrahydrofuran at 1 ml/min over 30 min. Polystyrene standards were utilized for calibration.

2.3 | Thermal analysis of PβAE polymer

Thermal gravimetric analysis (TGA) was performed on the dried polymer utilizing a Q50 Series TGA by TA Instruments utilizing a 10°C/min ramp in temperature. Differential scanning calorimetry was also

performed on the polymer with a DSC-Q2000 by TA Instruments. The method was a modulation occurring $\pm 0.5^{\circ}\text{C}$ every 60 s and started with an equilibration at -50°C and holding isothermally for 10 min. An increase in temperature to 150°C was done at 5°C/min and then held isothermally for 5 min to mark the end of cycle one. Cycle two consisted of rapid ramp down in temperature before performing the cycle 1 parameters for the final cycle.

2.4 Nanoparticle synthesis and characterization

The PBAE nanoparticles were synthesized through a facile precipitation method taking advantage of the soluble and hydrophobic nature of the bulk polymer. The polymer was solubilized in dimethyl sulfoxide (DMSO) and while stirring at 600 rpm, 250 µl of the polymer solution was added to 16 ml of DI H₂O. The resulting suspension was then immediately tested using dynamic light scattering (DLS). The DLS measurement was recorded with a refractive index of 1.590 and absorption of 0.010. Using an incidence angle of 90°, three measurements were taken with 10-12 runs per measurement. To test the effect of polymer concentration on nanoparticle size, 90CMA polymer solutions of varying concentrations (40, 20, 10, 5, and 2.5 mg/ml) in DMSO were utilized. To determine the effect of pH on zeta potential, 10 mg/ml 90CMA polymer solution was used to synthesize nanoparticles that were then dried overnight through lyophilization. The nanoparticles were resuspended in 1.5 ml of prepared Britton-Robinson buffer solution at various pHs (3, 5, 7, 9, and 11 with ionic strength equal to 0.1 M). Zeta potential was immediately run on the suspensions using three measurements with 10-30 runs per measurement.

2.5 | Dip coating of glass slides

The processability of the PβAE polymer was further demonstrated by synthesizing coatings using a 7.5 w/v% solution of 80CMA in DCM. A simple dip coating technique was utilized taking advantage of a 5 kN Instron Model 3345 to control the withdrawal speed. To determine the effect of withdrawal speed on final film thickness, withdrawal speeds were varied between 0.01 and 10 mm/s. The following parameters remained constant for each coating: dwell time of 10 s, dry time of 24 h, and an average coating height of about 12 mm. Single layer thin films were coated onto glass microscope slides (75 \times 25 \times 1 mm) and film thickness was determined using electron microscopy. A 20nm platinum coating was deposited at the surface of the samples to increase the electrical conductivity prior to electron microscopy characterization (EM ACE600 sputter coater, Leica Microsystems, Wetzlar, Germany). Cross-sectioning of the films and subsequent imaging was performed using a focused ion beam/scanning electron microscope system (Helios Nanolab 660/G3 dual beam from ThermoFisher Scientific/FEI, Hillsboro, OR, USA). Film thicknesses were directly determined from the cross-sectional images. Elemental composition of the films was determined using the same instrument, using energy dispersive x-ray spectroscopy (EDS, X-Max^N detector, Oxford Instruments,

Abingdon, United Kingdom). The viscosity of the polymer was determined by varying shear rates at 25°C through a microVISC (HVROC-T) from RheoSense.

2.6 | Inkjet printing of thin films

Inkjet printing of the PBAE polymer onto a glass slide was a second method for developing thin films. This technique utilized the Fujifilm Dimatix 2850 Inkjet Printer, a piezoelectric drop on demand inkjet printer. The ink was formulated by solubilizing the 80CMA polymer in DMSO at 5 w/v%. The solution was then passed through a 0.45 µm polytetrafluoroethylene (PTFE) filter for a final concentration of 4.4 w/v%. The ink was characterized through viscosity measurements on the RheoSense microVISC. In addition, surface tension (pendant drop) and contact angle with the substrate (sessile drop) were determined on the Drop Shape Analyzer from Krüss. The ink was then added to a new Dimatix printer cartridge containing 16 nozzles with 254 µm spacing and 10 pl jetted droplet volume. The substrate platen temperature was kept at 40°C with the printhead temperature at 60°C. A 7.5 mm \times 7.5 mm square was printed at 1016 drops per inch (dpi) for each sample. Each laver was dried under reduced pressure (>100 mbar) for 1 min. To analyze the effect of layering multiple thin films, successive layers were printed on dry base layers up to three total layers. The thickness of the layers was determined utilizing a Dektak 6 M Stylus Profilometer. The loading of curcumin on each slide was determined through solubilization of the printed layers in DMSO and subsequent analysis on UV-vis.

2.7 | Degradation studies

The release of the curcumin monomer from the bulk polymer, nanoparticles, and coatings was determined through degradation studies. The samples were placed in phosphate buffered saline (PBS, 1 wt% Tween80 at pH 7.4, and ionic strength 0.5 M) in a Thermo Scientific Precision SWB 15 shaker bath at 37°C and 130 rpm. Over a period of 14 days, at each time point 1 ml of sample was removed and replaced with 1 ml fresh PBS solution. The samples were then analyzed utilizing HPLC with the same method file as previously described. For bulk polymer and nanoparticle degradation, each sample was set up to have a theoretical curcumin loading of 50 $\mu\text{g/ml}$ in approximately 20 ml of buffer solution taking into account the varying curcumin loadings across the synthesized polymers. The dip coated and inkjet printed thin films were degraded utilizing a similar protocol with 10 ml of buffer solution and 0.5 ml of sample drawn each time point, except the theoretical loading was determined from the coating thickness and area.

2.8 | Trolox equivalent antioxidant capacity assay

The total antioxidant activity of the released degradation products of the bulk, nanoparticle, and thin film coatings were determined through a Trolox equivalent antioxidant capacity (TEAC) assay. Equivalent amounts of 8 mg/ml ABTS and 1.32 mg/ml PPS were mixed in the dark 12–16 h at room temperature before use to produce free radical ABTS. Trolox standard solutions or samples were added to the ABTS radical solution for 5 min and then read at 734 nm utilizing a UV-visible spectrophotometer microplate reader. A calibration curve was created utilizing the Trolox standards to allow for Trolox to be the reference antioxidant to determine the sample's antioxidant capacity, that is, the Trolox equivalence antioxidant concentration (mM).

3 | RESULTS

3.1 | Polymer synthesis and characterization

An organic soluble PBAE prodrug was synthesized through the one pot Michael addition of CMA, PEG400DA, and IBA (Figure 1B), CMA was successfully prepared as demonstrated through HPLC (Figure S1, Supporting Information) and the relative amounts of monoacrylate (4.0%), diacyrylate (75.6%), and triacrylate (20.4%) were determined. 18 The polymers of differing curcumin content (Table 1) were synthesized to determine the effect of curcumin content on varying properties. From GPC analysis, the polymeric molecular weight and polydispersity index, or PDI, were identified (Table 1, Figure S2, Supporting Information). Due to the nature of the measurement and the branched polymer, these values indicate a relative molecular weight respective to the standards and solvation in THF that was seen to increase with an increasing curcumin feed content. The 90CMA and 80CMA polymers exhibited similar conversions at the highest molecular weight indicating an upper limit under the current synthesis parameters. However, the 90CMA polymer showed a greater variance in polymer size as evidenced by the larger PDI. The polymers were purified through diethyl ether washes to remove any unreacted monomer and the purification was analyzed through GPC. Figure S3, Supporting Information, demonstrates the reduction in lower molecular weight moieties with an increased number of washes.

3.2 | Thermal analysis

Thermal gravimetric analysis (TGA) (Figure 2) was performed to determine the temperature stability of the synthesized polymers. As evidenced, the polymers were thermally stable up to 150° C at which point they begin to degrade. Rapid degradation begins to occur at 200° C and ending at 400° C. A slight increase in stability resulted from an increase in CMA content. DSC was also utilized to determine the glass transition temperature of the polymers (Figure 3, Figure S4, Supporting Information). The glass transition temperature indicates a transition in the polymer from a rigid state to a more flexible state. From Figure 3, it was seen that an increase in CMA content resulted in an increase in the T_g .

(B)

FIGURE 1 (A) The structure of the functionalized monomer from curcumin. For the monoacrylate form, only X, Y, or Z is an acrylate group with the remaining groups being hydrogens. For the diacrylate form, X, Y, or Z remains a hydrogen with the other two groups forming acrylates. For the triacrylate form, all three groups are acrylates. For all acrylate structures R_1 and R_2 are OCH $_3$ if derived from curcumin, H and OCH $_3$ if derived from demethoxycurcumin, and both H if derived from bisdemethoxycurcumin. (B) Depicts the polymerization scheme showing the addition of the curcumin diacrylate to represent CMA with PEG400DA in various ratios with the amine IBA to synthesize the bulk PβAE polymers

TABLE 1 Compositions of curcumin P β AE polymers synthesized at a ratio of total acrylate to amine protons of 0.8

	Molar acrylate ratio CMA:PEG400DA	CMA content (wt%)	Molecular weight (MW)	PDI
90 CMA	90:10	54%	30,000	4.52
80 CMA	80:20	48%	29,000	4.07
70 CMA	70:30	42%	16,000	2.81
60 CMA	60:40	36%	13,000	2.29
50 CMA	50:50	30%	8000	1.95

Notes: The molecular weight and polydispersity index data were gathered utilizing GPC.

3.3 | Bulk degradation and antioxidant activity

To determine the impact of the comonomer ratio on degradation, a series of aqueous degradation studies was performed. To monitor the degradation, the bulk P β AEs were submerged into PBS solution with 1 wt% Tween 80. Samples were collected at specified time points and analyzed through an HPLC with an UV-visible detector at 420 nm. The active release products were determined to be curcumin and curcumin monoacrylate. As demonstrated in the bulk polymer degradation profile, the higher curcumin weight loadings resulted in an increased release of curcumin (Figure 4A). The 80CMA polymer exhibited the highest curcumin release with 14 μ g/ml and a recovery of

28% based on the theoretical loading over the 14-day degradation period. The lower curcumin weight loading at 50CMA exhibited the lowest curcumin release at 4 ug/mL and 8% recovery during the same

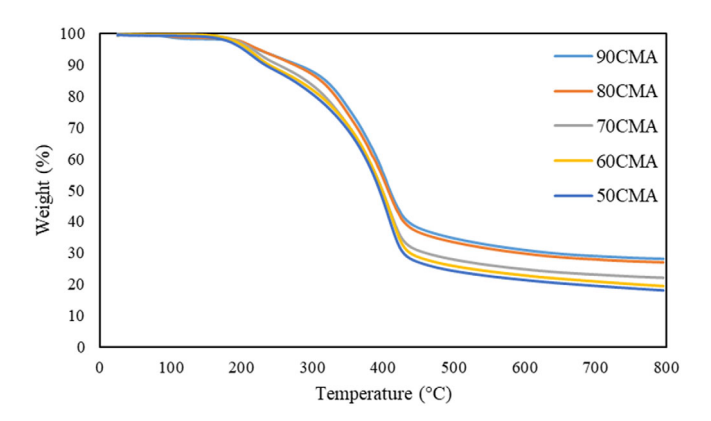


FIGURE 2 Thermogravimetric analysis of the varying curcumin $P\beta AE$ bulk polymers. With an increase in curcumin content there was an increase in the overall decomposition temperature.

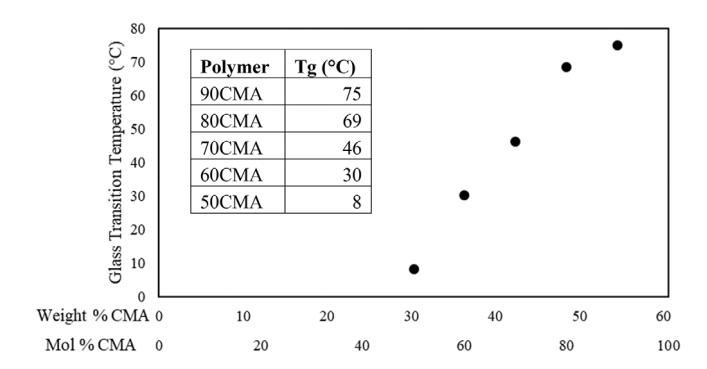


FIGURE 3 Plot of the glass transition temperature versus the weight and mol percent of curcumin multiacrylate from differential scanning calorimetry for the varying curcumin P β AE bulk polymers. The inset table contains the exact glass transition temperatures.

time frame. As seen in Figure S3, Supporting Information, less than or equal to 2% of the theoretical loading was curcumin monoacrylate released indicating that the primary active product was the original reactant curcumin. Minimal release of CMA was advantageous due to the limited knowledge on the toxicity of the monomer. Further analysis is required to determine the threshold for maximum monoacrylate release. Additionally, complete hydrolysis and release of the polyphenol was ideal on account of the inherent superior antioxidant activity of curcumin. Curcumin release began on day 2 after the hydrophobic polymer could be sufficiently penetrated by water to begin the hydrolysis reaction. As seen in the TEAC assay, the antioxidant activity of the bulk polymers followed the pattern of curcumin release (Figure 4B). The 80CMA polymer exhibited the highest antioxidant activity on day 13 with a TEAC of 0.29 mM and the lowest TEAC was the 50CMA polymer at 0.16 mM. As with the curcumin release profile, the antioxidant activity was shown to increase over time as the degradation of the polymers progressed.

3.4 | Polymer processing and characterization

Since the bulk $P\beta AE$ polymers were synthesized to have a branched but not crosslinked structure, they were found to be soluble in organic solvents. The $P\beta AE$ polymer's solubility was determined and controlled through the incorporation of the various monomers. To take advantage of this solubility the polymers were further developed into nanoparticles and thin films. The nanoparticles were synthesized through the condensation method. Briefly, 90CMA polymer at varying concentrations was solubilized in dimethyl sulfoxide and added to deionized (DI) water. Due to the miscibility of the water and organic solution, the hydrophobic polymer was then condensed into a nanoparticle. The nanoparticle size was determined through dynamic light scattering and was found to increase with increasing polymeric concentration (Figure 5). The polydispersity index was also determined to indicate the size distribution of the particles. The lowest curcumin weight loading of 50CMA indicated a size of 80 nm and the highest

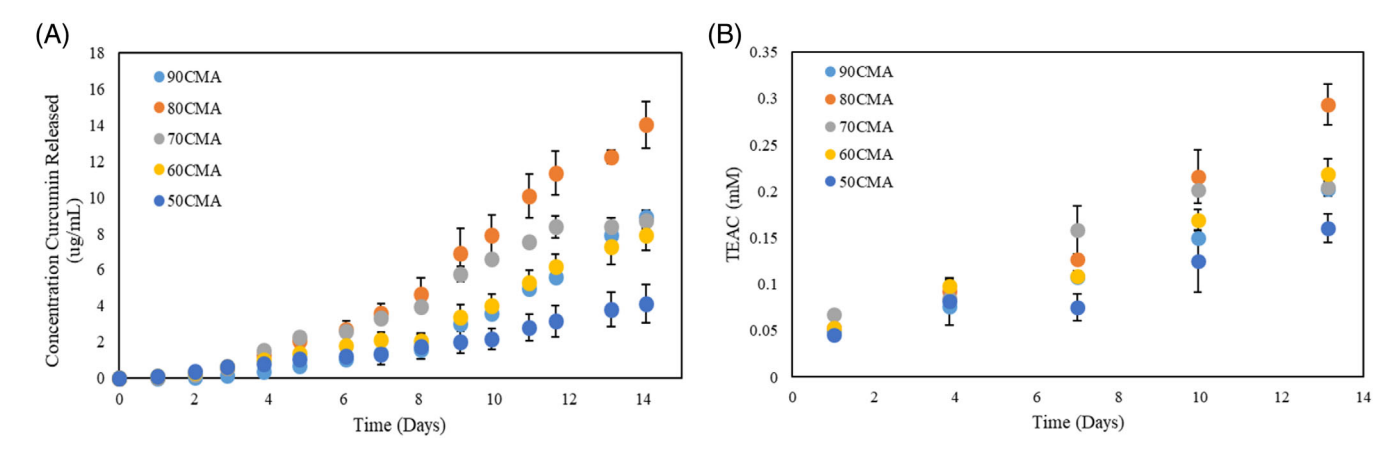


FIGURE 4 (A) Release profiles of curcumin from varying curcumin loaded PβAE bulk polymers in PBS, 1 wt% Tween80 (mean \pm SEM, n=3). (B) Trolox equivalence antioxidant concentration (TEAC, mM) for the varying curcumin loaded PβAE bulk polymers in PBS, 1 wt% Tween80 (mean \pm SEM, n=3). Direct comparison of the two plots can be seen in Figure S6, Supporting Information.

curcumin loading of 90CMA had a size of 160 nm with a greater PDI indicating agglomeration. The PDI was shown to fluctuate between 0.2 and 0.3 suggesting minimal agglomeration, particularly for the polymeric concentrations below 20 mg/ml.

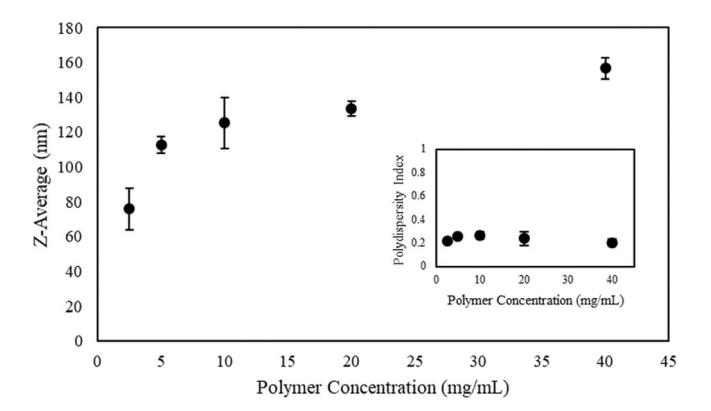


FIGURE 5 Plot of the z-average representing nanoparticle size versus the concentration of the 90CMA bulk polymer (mean \pm SEM, n=3). The inset figure depicts the corresponding polydispersity index (mean \pm STDEV, n=3).

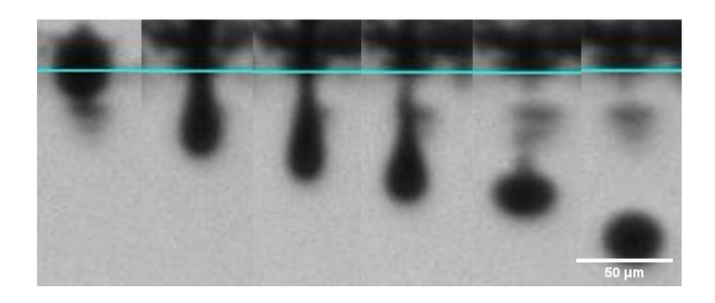
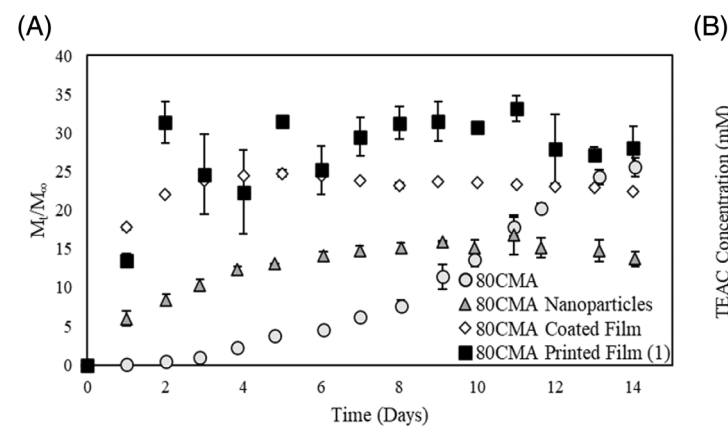


FIGURE 6 Image of the drop formation of the 5 wt% 80CMA polymer solubilized in DMSO. Individual drop images taken every 5 μ s over a 30 μ s period.

Thin coatings were synthesized through a simple dip coating technique to demonstrate the versatility of the organic soluble P β AEs. The coating thickness was controlled by varying the withdrawal speed. The thickness was determined through scanning electron microscopy and the location of the polymer layer was confirmed through EDS (Figure S5, Supporting Information). The experimental values were then utilized in various models based off the withdrawal speed to characterize the coating regimes (Figure 9A).

While dip coating allowed for the simple fabrication of single P β AE layered films, inkjet printing facilitated the synthesis of multiple layered films. These layers were fabricated through multiple passes on the inkjet printer after complete drying of the previous layer. The ejected ink droplets were shown to have good wettability on the both the initial glass substrate and subsequent dried polymer layers as demonstrated by the contact angles of 14.8° and 20.3° respectively (Figure S7, Supporting Information). The viscosity of the ink was optimized at a 5 wt% C80 polymer solution in DMSO (Figure S6b, Supporting Information) and filtered to help prevent nozzle clogging. Drop formation (Figure 6) was achieved through waveform optimization (Figure S8, Supporting Information) and a cartridge temperature of 60°C to help prevent agglomeration at the nozzle printhead.

The polymer was then printed in 7.5×7.5 mm squares with a drop spacing of 1016 dpi to aid the formation of a homogenous film. Due to strong Marangoni flow during drying that caused an inhomogeneous film when drying in ambient conditions, the printed polymer was flash dried under reduced pressure. While the films printed evenly in the outlined square, interactions of the printed pattern with fast-moving air caused some film inconsistencies during flash drying (Figure S9, Supporting Information). The thickness of these final printed films was analyzed through profilometry to determine the average thickness of the polymeric films. As expected, the thickness of the printed films increased with each subsequent layer: one layer (455 \pm 3 nm); two layers (677 \pm 5 nm); and three layers (1392 \pm 9 nm).



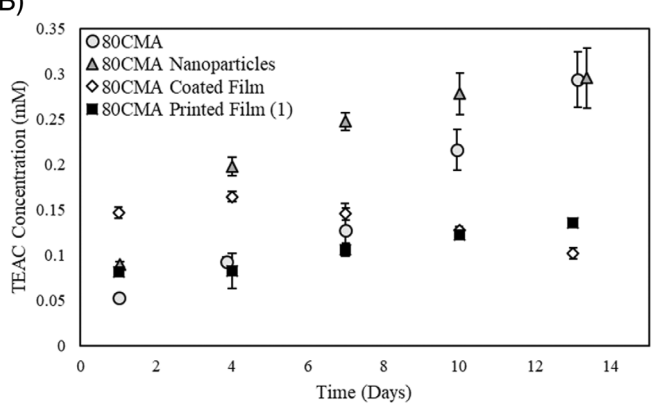


FIGURE 7 (A) Release profiles of curcumin 80CMA bulk polymer (circles), nanoparticles (triangles), coated films (diamonds), and single layer printed films (squares) in PBS, 1 wt% Tween80 where M_{∞} was equivalent to complete theoretical release (mean ± SEM, n=3). (B) Trolox equivalence antioxidant concentration (TEAC, mM) for 80CMA bulk polymer (circles), nanoparticles (triangles), coated films (diamonds) and single layer printed films (squares) in PBS, 1 wt% Tween80 (mean ± SEM, n=3)

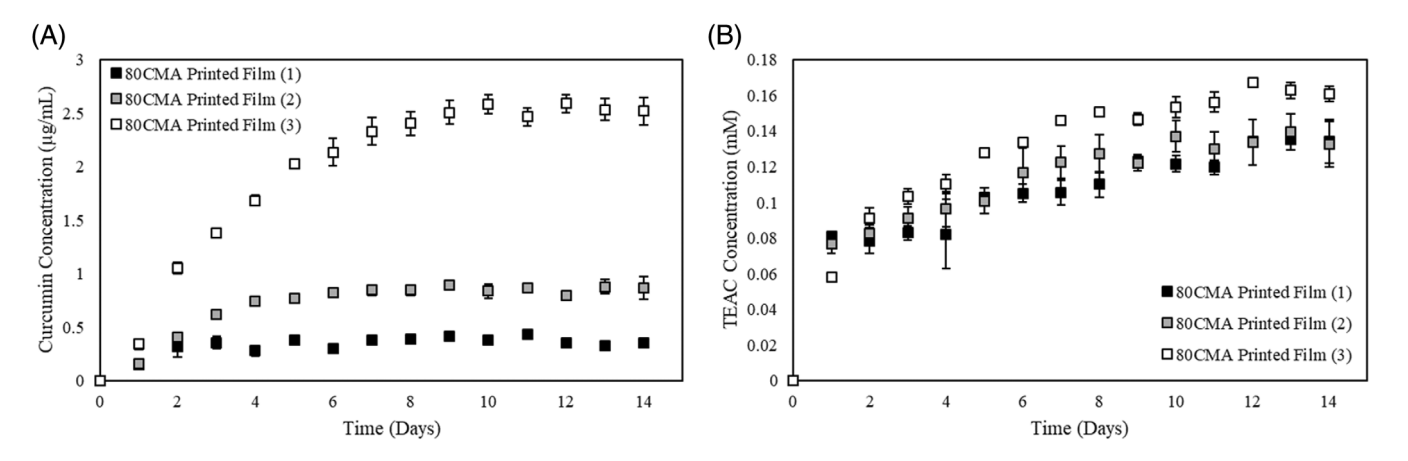


FIGURE 8 (A) Release profiles of total curcumin concentration from printed 80CMA single film (black), double layered (gray), and triple layered (white) films in PBS, 1 wt% Tween80 (mean \pm SEM, n=3). (B) Trolox equivalence antioxidant concentration (TEAC, mM) for printed 80CMA single film (black), double layered (gray), and triple layered (white) films in PBS, 1 wt% Tween80 (mean \pm SEM, n=3)

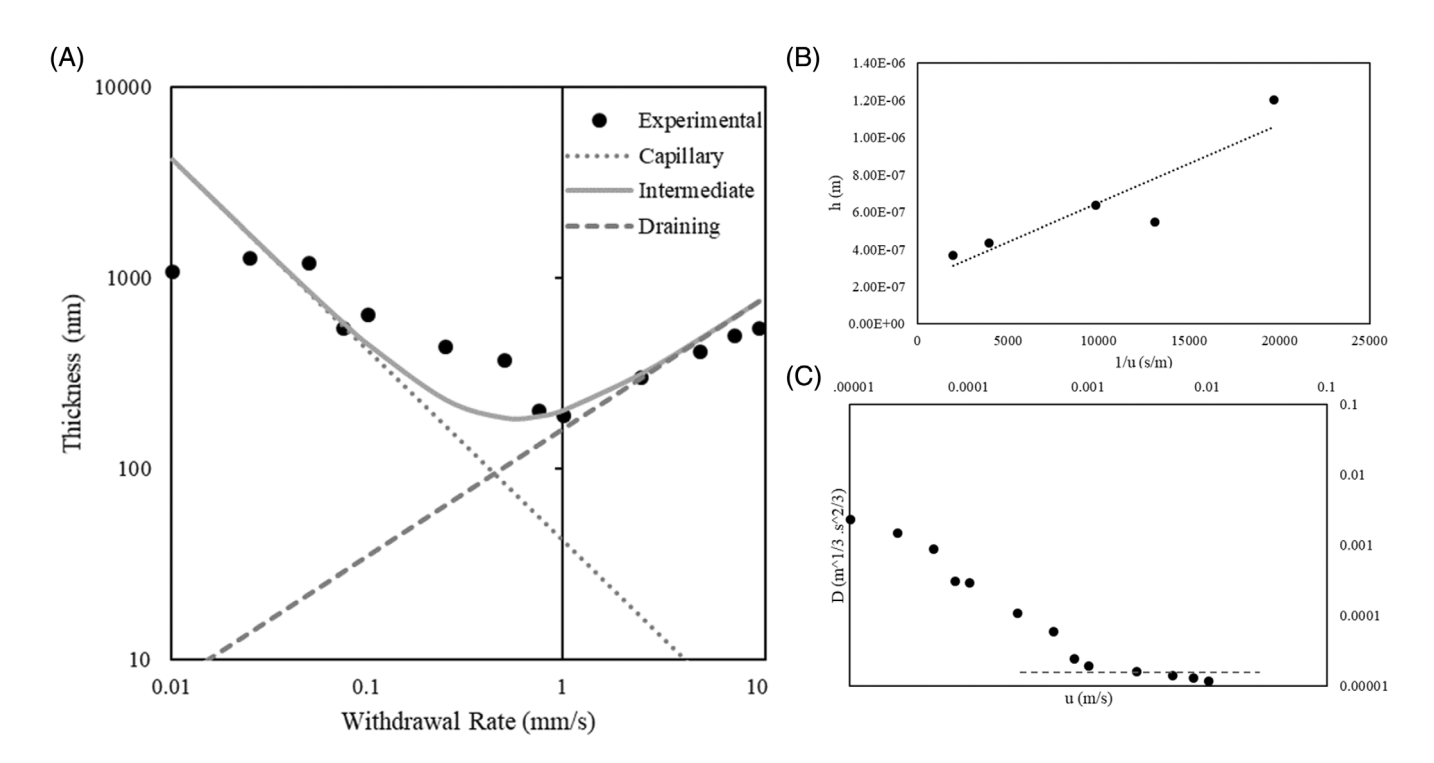


FIGURE 9 (A) Plot of the 80CMA thin-film thickness versus the withdrawal rate (log-log scale) for the experimentally determined points and corresponding models for the separate (dashed lines) and the combined (solid line) regimes. (B) h_0 versus 1/u plot (experimental points and corresponding capillary model). (C) D versus u plot (log-log scale) highlighting the draining regime (dashed line)

3.5 | Degradation and antioxidant activity from processed PβAEs

Degradation studies were performed on the nanoparticles and thin films to demonstrate the release of curcumin relative to the polymer structure. TEAC assays were also performed to confirm the processing procedures did not alter the polyphenol's antioxidant activity. Nanoparticle degradation was performed similarly to the bulk 80CMA polymer release studies. Nanoparticles synthesized from 80CMA polymer at a concentration of 10 mg/ml with an initial size of 150.4 ± 10.2 nm

were lyophilized and resuspended in DI water. After analysis through DLS, the size was determined to be 169.4 ± 0.3 nm indicating slight agglomeration of the nanoparticles after drying. The nanoparticles were then submerged in neutral phosphate buffer with 1 wt% Tween 80. The 80CMA nanoparticles indicated a more rapid release of curcumin with 6% release of the theoretical loading beginning on day 1 compared to the bulk 80CMA polymer which exhibited 0.5% curcumin release on day 2 (as seen in Figure 7A). Peak release for the nanoparticles was reached on day 9 at 16% curcumin released compared to peak release for the bulk polymer on day 14 at 26%. The quicker

curcumin release from the nanoparticles resulted in a higher antioxidant capacity during the earlier degradation period which can be seen in Figure 7B. On day 1, the nanoparticle TEAC response was 0.09 mM, and the bulk polymer was 0.05 mM. By day 13, the nanoparticles and bulk polymer exhibited a similar TEAC response of approximately 0.3 mM.

Degradation was performed similarly to the bulk and nanoparticle systems to characterize the curcumin release from the 80CMA polymeric dip coatings. Coated films with a thickness of 410 nm were synthesized on glass slides utilizing a withdrawal speed of 5.08 mm/s. The coated glass slides were then submerged into PBS supplemented with 1 wt% Tween80 for the release studies. The 80CMA coatings demonstrated a rapid release of curcumin with 18% released on day 1 and peak release of about 25% of the theoretical loading was reached on day 5 as seen in Figure 7A. Likewise, the inkjet printed single layer films demonstrated a more rapid release compared to that of the bulk polymer or nanoparticles. The single layer films were fabricated through printing of the 5 wt% polymeric ink at 60°C at 1016 dpi. The printed films were dried under reduced pressure and placed into PBS with 1 wt% Tween80. The 455-nm thick printed single layer films demonstrated a similar release profile to the dip coated films. An initial release of 13% was observed from the printed films on the first day with approximately 30% curcumin release observed throughout the remainder of the study (Figure 7A). Since both thin films demonstrated a guicker curcumin release than the nanoparticles and bulk polymer, the antioxidant capacity was greater. A TEAC response of 0.15 and 0.08 mM was observed on day 1 for the coated and printed films, respectively (Figure 7B). However, by day 13 the TEAC response had decreased to 0.10 and 0.13 mM as the rate at which the films were releasing curcumin had decreased.

Curcumin release and antioxidant activity was also analyzed from the multiple layer inkjet printed $P\beta AE$ films. As expected with each subsequent layer of printed film, an increase in curcumin release was observed (Figure 8A). Due to the spreading of the films during the drying stage, the correlation between number of layers and amount of curcumin released deviated from linearity. Similarly, an increase in antioxidant activity was observed with an increase in number of printed layers due to an increased deposition of curcumin on the glass slide (Figure 8B).

4 | DISCUSSION

4.1 | Increasing curcumin content, increases polymer molecular weight and chain branching

For the polymer synthesis, the CMA monomer was chosen as the active ingredient for the antioxidant potential associated with curcumin. PEG400DA was included as a hydrophilic comonomer due to the hydrophobic nature of curcumin and to help provide control over degradation rates. Crosslinking during polymerization occurs when the aggregate monomer functionality exceeds two. Due to the fact that CMA is a triacrylate, the polymer was able to form a more branched structure. To reduce the network functionality, we focused on amine

reactants which were bifunctional. The primary amine, IBA, was chosen to facilitate the development of a branched or linear polymer due to the proximity of its reactive groups. The structure of IBA had a high degree of steric hindrance which limited the degree of branching. Table 1 shows the effect of curcumin content on the resulting polymers. A general trend of increasing relative molecular weight was observed with increasing curcumin content. However, at the highest curcumin incorporation, there was an increase in the branching of the polymer, restricting the extent of synthesis. During bulk polymerization, the increase in branching results in an increase in steric hindrance that reduces further polymerization. This increase in branching was a result of the overall increase in triacrylate content and was reflected in a general increase in PDI as the polymers with a greater curcumin content exhibited less uniformity in the polymer size distribution.

4.2 | Curcumin content improves thermal stability

The two-step degradation observed in Figure 2 at approximately 200°C and ending at approximately 400°C was a consequence of the decomposition of the monomer CMA. As evidenced in previous literature, CMA exhibits a two-step degradation suggesting in the first stage the substituent groups undergo decomposition while the two benzene rings decompose during the second stage similar to the curcumin monomer. 18,36 These results indicate that processing temperatures for these polymers would need to be below 150°C to retain polymer integrity. As with many drugs, the processing temperatures are often limited by the active ingredient. At the upper limit of the polymer, curcumin exhibits degradation and reduction in activity thus limiting processing temperatures. 36,37 The increase in T_g with increasing CMA content observed in Figure 3 was a result of the flexibility of the individual monomeric units that constituted the polymeric backbone. Compared to PEG400DA, CMA has a relatively short and stiff structure. Therefore, polymers high in CMA content have more rigid chains. Additionally, the increased CMA content corresponded to an increased polymeric branching. The branching requires an increased amount of energy to push the chains into the rubbery state due to the increased number of entanglements per chain. The combination of increased structure rigidity and branching account for the rapid rise in glass transition temperature.

4.3 | Control over nanoparticle size and thin-film formation

The synthesis of nanoparticles from the bulk P β AE polymers was possible due to the inherent properties of the polymers. The structure of the polymer facilitated its solubility in organic solvents and the use of a simple precipitation method for nanoparticle formation. The increasing size trend observed in Figure 5 is common for nanoparticles formed through this method as the higher polymer concentration condenses into larger particles. This work demonstrates by varying the polymeric concentration, nanoparticle size can be controlled to suit specific applications. Particle size has been shown to affect clearance

rates, circulation time, drug release profiles, etc.³⁸ Exhibition of control over size through nanoparticle synthesis is crucial to achieve optimal treatment efficiency.

Thickness of the dip coated films determined through SEM was utilized to characterize the coating regimes through models based off withdrawal speed (Figure 9A). At very low withdrawal speeds (0.01–0.1 mm/s), the capillary regime is dominated by the solvent evaporation and final film thickness (h) can be determined through Equation (1).³⁹

$$h = \frac{E}{I \times u} \tag{1}$$

E is the rate of solution evaporation. L is the film width, and u is the withdrawal rate of the substrate from polymer dope solution. In this regime, the evaporation of the solvent is faster than the movement of the drying line which results in a continuous feeding of the upper part of the meniscus through capillary rise.⁴⁰ When the capillary regime dominates, the h_0 versus 1/u plot results in a straight line with the slope corresponding to the solution consuming rate (E/L) (Figure 9B). The deviation in experimental values from the model at extremely low withdrawal speeds is attributed to the volatility of the solvent used in the dope solution. Since the model equations depicted in Figure 9A assumed Newtonian and nonvolatile solutions, the volatility of DCM in the polymer dope solution greatly exacerbates the dominating effect of the evaporation. The polymer solution was determined to be Newtonian at higher shear rates indicating that the lower withdrawal speeds are subject to greater deviation from the modeling equations (Figure S6a, Supporting Information). At higher withdrawal speeds (1-10 mm/s), the coating thickness can be described by the Landau and Levich equation. This draining regime is characterized by the ratio of viscous and capillary forces as evidenced in Equation (2).41

$$h = D \times u^{\frac{2}{3}}; D = 0.94 \frac{n^{2/3}}{\gamma^{1/6} (\rho g)^{1/2}}$$
 (2)

D represents a global constant composed of the constant for flat substrates, standard gravity, and the viscosity (η), surface tension (γ), and density (ρ) of the polymer solution. The validity of this model in this region was verified by the constant D value at the higher withdrawal speeds exhibited by plotting D versus withdrawal speed, u (Figure 9C). At the greatest withdrawal rates, a slight decrease was evidenced in D. This deviation was attributed to the inability to counterbalance the increasing thickness of the deposited layer with the adhesion to the surface. At intermediate withdrawal speeds (0.1–1 mm/s), both regimes of coating formation are overlapping and therefore the models can be combined as seen in Equation (3).

$$h = \left(\frac{E}{L \times u} + D \times u^{\frac{2}{3}}\right) \tag{3}$$

The slight deviation from the intermediate model can again be attributed to the volatility of the solvent resulting in a greater influence by the capillary regime. The synthesis of the nanoparticles and thin films demonstrated the benefits of developing a soluble P β AE prodrug system while still maintaining control over the processing procedures through conventional methods. The previous thermoset network could not have been manipulated in such a manner.

Multiple passes with an inkjet printer facilitated the fabrication of multiple layer $P\beta AE$ films. The thickness of these films was determined to increase with each subsequent layer. However due to the spreading of the films that occurred during drying, the linear increase in thickness deviated slightly. The generation of stable droplets is a complex process, but fluid properties can help determine a printable ink. In general, the behavior of an ink during inkjet printing can be described using the following dimensionless parameters:

$$Reynolds(Re) = \frac{v\rho a}{\eta},$$
 (4)

Weber (We) =
$$\frac{v^2 \rho a}{\gamma}$$
, (5)

Ohnesorge (Oh) =
$$\frac{\sqrt{\text{We}}}{\text{Re}} = \frac{\eta}{\sqrt{(\gamma \rho a)}}$$
, (6)

where ρ , η , and γ are the density, dynamic viscosity, and surface tension of the fluid respectively with v being the velocity and a being the diameter of the ejected droplet.⁴² For determining stable drop formation, the fluid velocity independent dimensionless parameter Z is often used⁴³:

$$Z = \frac{1}{Oh} = \frac{Re}{\sqrt{We}} = \frac{\sqrt{(\gamma \rho a)}}{\eta}.$$
 (7)

Previous work has utilized computation fluid dynamics modeling to determine the limits of Z to be $1 < Z < 10.^{42-45}$ At the lower bound, Z is limited due to viscous dissipation preventing proper drop ejecting. At the upper bound, Z is limited due to the formation of satellite drops. For this work, Z was determined to be 6.3 indicating stable drop formation. In order for drop ejection, the drop must have sufficient energy to overcome the viscous and surface tension forces during drop formation. This energy is supplied by the actuating pulse and a minimum velocity must be achieved which can be defined by a We >1 for drop formation. 42,43 The We was determined to be 5.8 indicating sufficient fluid velocity to facilitate drop formation. In addition, the ejected drop on the substrate must impact as to leave an isolated spread drop. The threshold for the onset of splashing has been proposed as a grouping of dimensionless variables 42,46,47 :

$$We^{0.5}Re^{0.25} > f(R),$$
 (8)

where f(R) is a function of surface roughness only. For flat, smooth surfaces f(R) is approximately equal to 50.^{42,48} Due to the relatively low We and Re numbers of 5.8 and 15.2, respectively, splashing did not occur and the final equilibrium film shape was controlled through capillary spreading. Additionally, the polymer was heated to an



elevated temperature of 60° C allowing for an increased viscosity and mobility of the polymer without initiating thermal degradation of the active ingredient curcumin. This helped prevent aggregation of the polymer at the nozzle head and facilitate smooth formation of droplets.

4.4 | Processing determined release and antioxidant activity from PβAEs

Due to polymeric degradation proceeding through hydrolysis at the ester bond, a dependency was created on the hydrophobic nature of the polymer. Therefore, the ratio of the incorporation of the hydrophobic monomer (CMA) to the hydrophilic monomer (PEG400DA) controlled the rate of release of curcumin. This phenomenon was seen in the bulk polymer degradation profile with greater curcumin loadings resulting in an increased curcumin release (Figure 4A). As the reaction continued forward and the breakdown of the polymers transitioned into oligomers, the rate of degradation increased allowing for an increased release of curcumin over time. As demonstrated by the TEAC assay, the retention of the native curcumin activity was retained through polymerization of the soluble $P\beta AE$ system and mimicked that of the curcumin release (Figure 4B).

Additionally, degradation studies and TEAC assays were utilized to determine the effect of processing procedures on the curcumin release from nanoparticles and thin films. A more rapid curcumin release was observed (as seen in Figure 7A) and can potentially be attributed to an increase in the surface area to volume ratio allowing for an increased penetration of water to begin the hydrolysis reaction. The 80CMA bulk polymer had a slight delay in curcumin release as the water had to penetrate the hydrophobic polymer to begin hydrolysis. The same reaction occurs during nanoparticle degradation, but the increase in surface area allows for a reduction in the delay of curcumin release. As expected, Figure 7B demonstrated a greater antioxidant capacity earlier in the degradation period for the nanoparticles. The accelerated curcumin release and corresponding antioxidant capacity could be beneficial as it allows for quicker entry into the therapeutic window and more immediate free radical scavenging capabilities.

The release of both the dip coated and inkjet printed films was much quicker than the 80CMA nanoparticles and bulk polymer indicating the rate of hydrolysis at the ester bonds could not solely be attributed to the increase in the surface area to volume ratio. The increased rate of curcumin release from the coatings could be a result of porosity in the films. The increased surface area coupled with the porosity of the coatings allowed for the increased water penetration and subsequent ester hydrolysis releasing curcumin. As with the other systems, the increased curcumin release resulted in an increased antioxidant response. The processed systems demonstrated a release of curcumin dependent upon structure and exhibited an antioxidant activity corresponding to the overall release of degradation products.

5 | CONCLUSIONS

Soluble curcumin conjugated polyphenolic P β AE systems were synthesized and shown to successfully release curcumin through hydrolysis at the ester bonds. These bulk polymers were further processed into nanoparticles and thin films, a feat that had previously been accomplished with linear P β AEs and not for the delivery of polyphenols. Control was exhibited over the nanoparticle size and film thickness through polymer solution concentration and withdrawal speed respectively. In addition, multilayer films were fabricated through inkjet printing. Curcumin release and retention of antioxidant activity was characterized and demonstrated through release studies and TEAC assays for the bulk polymer, nanoparticles, and thin films. Interestingly, the processing of the polymer impacted the release profile of the P β AE polymer. The films and nanoparticles demonstrated a more rapid curcumin release and quicker antioxidant activity resulting from the increased surface area.

This work integrates the ability to maintain the beneficial drug delivery properties of P β AE systems combined with the discovery of an organic soluble P β AE structure. This allows for the controlled and tunable delivery of the active ingredient while facilitating polymer processing. To demonstrate the polymer processability, the bulk curcumin P β AE was synthesized into nanoparticles and thin films. However, the polymer could be solubilized into a gel, spun into nanofibers, or solvent casted into a layered film system. The improved processability of the organic soluble P β AE increases the realm of potential applications.

ACKNOWLEDGMENTS

This work was funded through a grant from the NIH SBIR (R44DE023523), a Kentucky State Matching Grant, and the National Science Foundation (1849213). Access to characterization instruments and staff assistance was provided by the Electron Microscopy Center at the University of Kentucky, member of the National Nanotechnology Coordinated Infrastructure (NNCI), which was supported by the National Science Foundation (ECCS-K1542164).

CONFLICT OF INTEREST

The authors of this work have equity, ownership in, and serve as advisors for Bluegrass Advanced Materials, LLC which is currently developing products related to the research being reported. The terms of this arrangement have been reviewed and approved by the University of Kentucky in accordance with its responsible conduct of research policies.

DATA AVAILABILITY STATEMENT

The data that support the findings of this study are available from the corresponding author upon reasonable request.

ORCID

Kelley Wiegman https://orcid.org/0000-0002-4180-9012

REFERENCES

- Tsung J, Burgess DJ. In: Siepmann JSRA, Rathbone MJ, eds. Fudamentals and Applications of Controlled Release Drug Delivery. Springer; 2012:107-123.
- Sung YK, Wan Kim S. Recent advances in polymeric drug delivery systems. Biomater Res. 2020;24:1-12.
- Dhaliwal K, Dosanjh P. Biodegradable polymers and their role in drug delivery systems. Biomed J Sci Tech Res. 2018;11:8315-8320.
- Liechty WB, Kryscio DR, Slaughter BV, Peppas NA. Polymers for Drug Delivery Systems. Annu Rev Chem Biomol Eng. 2010;1:149-173.
- Brannon-Peppas L. Polymers in controlled drug delivery. Med Plast Biomater. 1997;V4:34-44.
- Mojzer EB, Hrncic MK, Skerget M, Knez Z, Bren U. Polyphenols: extraction methods, Antioxidative action, bioavailability and Anticarcinogenic effects. *Molecules*. 2016;21:901-939.
- Chen L, Cao H, Xiao J. Polyphenols: Absorption, bioavailability, and metabolomics. In: Galanakis C, ed. Polyphenols: Properties, Recovery, and Applications. Vol 1. Woodhead Publishing; 2018:45-67.
- 8. Parisi IO, Puoci F, Restucci D, Farina F, Iemma F, Picci N. Polyphenols and their formulations: different strategies to overcome the drawbacks associated with their poor stability and bioavailability. In: Watson RR, Preedy VR, Zibadi S, eds. *Polyphenols in Human Health and Disease*. Vol 1. Academic Press; 2014:29-45.
- Nichols JA, Katiyar SK. Skin photoprotection by natural polyphenols: anti-inflammatory, antioxidant and DNA repair mechanisms. Arch Dermatol Res. 2010;302:71-83.
- Dehkharghanian M, Lacroix M, Vijayalakshmi MA. Antioxidant properties of green tea polyphenols encapulsated in caseinate beads. *Dairy Sci Technol*. 2009;89:485-499.
- Gupta P, Jordan CT, Mitov MI, Butterfield DA, Hilt JZ, Dziubla TD. Controlled curcumin release via conjugation into PBAE nanogels enhances mitochondrial protection against oxidative stress. Int J Pharm. 2016;2:1012-1021.
- Aquilano K, Baldelli S, Rotilio G, Ciriolo MR. Role of nitric oxide synthases in Parkinson's disease: a review on the antioxidant and anti-inflammatory activity of polyphenols. *Neurochem Res.* 2008;33: 2416-2426.
- Daglia M. Polyphenols as antimicrobial agents. Curr Opin Biotechnol. 2012;23:174-181.
- Zern TL, Fernandez ML. Cardioprotective effects of dietary polyphenols. J Nutr. 2005;135:2291-2294.
- Jordan CT, Hilt JZ, Dziubla TD. Polyphenol conjugated poly(betaamino ester) polymers with hydrogen peroxide triggered degradation and active antioxidant release. J Appl Polym Sci. 2019;137:48647.
- Liu Y, Li Y, Keskin D, Shi L. Poly(B-amino esters): synthesis, formulations, and their biomedical applications. Adv Healthcare Mat. 2019;8:
- Huang X, Liao W, Xie Z, Chen D, Zhang CY. A pH-responsive prodrug delivery system self-assembled from acid-labile doxorubicin-conjugated amphiphilic pH-sensitive block copolymers. *Mater Sci Eng C*. 2018;90:27-37.
- Patil VS, Gutierrez AM, Sunkara M, et al. Curcumin Acrylation for biological and environmental applications. J Nat Prod. 2017;80:1964-1971.
- Jordan CT, Hilt JZ, Dziubla TD. Modeling the oxidative consumption of curcumin from controlled released poly(beta-amino ester) microparticles in the presence of a free radical generating system. *Regen Biomat*. 2019;6:201-210.
- Patil VS, Dziubla TD, Kalika DS. Static and dynamic properties of biodegradable poly(antioxidant B-amino ester) networks based on incorporation of curcumin multiacrylate. *Polymer*. 2015;75:88-96.
- Wattamwar PP, Biswal D, Cochran DB, et al. Synthesis and characterization of poly(antioxidant *B*-amino esters) for controlled release of polyphenolic antioxidants. *Acta Biomater*. 2012;8:2529-2537.

- 22. Agrawal S, Goel RK. Curcumin and its protective and therapeutic uses. *Natl J Physiol Pharm Pharmacol*. 2016;6:1-8.
- 23. Sharma RA, Gescher AJ, Steward WP. Curcumin: the story so far. *Eur J Cancer*. 2005;41:1955-1968.
- Jayaprakasha GK, Jaganmohan Rao L, Sakariah KK. Antioxidant activites of curcumin, demethoxycurcumin, and bisdemethoxycurcumin. Food Chem. 2006;98:720-724.
- Nelson KM, Dahlin JL, Bisson J, Graham J, Pauli GF, Walters MA. The essential medicinal chemistry of curcumin. J Med Chem. 2017;60: 1620-1637.
- Yu Y, Zhang X, Qiu L. The anti-tumor efficacy of curcumin when delivered by size/charge-changing multistage polymeric micelles based on amphiphilic poly(B-amino ester) derivatives. *Biomaterials*. 2014;35:3467-3475.
- Gupta P, Authimoolam SP, Hilt JZ, Dziubla TD. Quercetin conjugated poly(B-amino esters) nanogels for the treatment of cellular oxidative stress. Acta Biomater. 2015;27:194-204.
- Akinc A, Anderson DG, Lynn DM, Langer R. Synthesis of poly(Bamino ester)s optimized for highly effective gene delivery. Bioconjug Chem. 2003;14:979-988.
- Anderson DG, Akinc A, Hossain N, Langer R. Structure/property studies of polymeric gene delivery using a library of poly(B-amino esters). Mol Ther. 2005;11:426-434.
- Anderson DG, Lynn DM, Langer R. Semi-automated synthesis and screening of a large library of degradable cationic polymers for gene delivery. Angew Chem Int Ed. 2003;42:3153-3158.
- Bhise NS, Gray RS, Sunshine JC, Htet S, Ewald AJ, Green JJ. The relationship between terminal functionalization and molecular weight of a gene delivery polymer and transfection efficacy in mammary epithelial 2-D cultures and 3-D organotypic cultures. *Biomaterials*. 2010;31: 8088-8096.
- Green JJ, Langer R, Anderson DG. A combinatorial polymer library approach yields insight into nonviral gene delivery. Acc Chem Res. 2008:41:749-459.
- Liu S, Gao Y, Sigen A, et al. Biodegradable highly branched poly(Bamino Ester)s for targeted cancer cell gene transfection. ACS Biomater Sci Eng. 2017;3:1283-1286.
- Gao Y, Huang JY, O'Keeffe Ahern J, et al. Highly branched poly(Bamino esters) for non-viral gene delivery: high transfection efficiency and low toxicity achieved by increasing molecular weight. *Biomacro*molecules. 2016;17:3640-3647.
- Zhou D, Cutlar L, Gao Y, et al. The transition from linear to highly branched poly(B-amino ester)s: branching matters for gene delivery. Sci Adv. 2016;2:1-14.
- Chen Z, Xia Y, Liao S, et al. Thermal degradation kinetics study of curcumin with nonlinear methods. Food Chem. 2014;155:81-86.
- Sun J-L, Ji H-F, Shen L. Impact of cooking on the antioxidant activity of spice turmeric. Food Nutr. 2019;63:3451-3457.
- Safari, H.; Kin-Hun Lee, J.; Eniola-Adefeso, O., Effects of shape, rigidity, size, and flow on targeting. In *Nanoparticles for Biomedical Applications*, Ji Chung, E. L., L.; Rinaldi, C., Ed. Elsevier: 2019; pp. 55–66.
- Brinker JC. Dip coating. In: Schneller TWR, Kosec M, Payne D, eds. Chemical Solution Deposition of Functional Oxide Thin Films. Springer; 2013:233-261.
- Faustini M, Louis B, Albouy PA, Kuemmel M, Grosso D. Preparation of sol-gel films by dip-coating in extreme conditions. J Phys Chem C. 2010;114:7637-7645.
- 41. Rio E, Boulogne F. Withdrawing a solid from a bath: how much liquid is coated? *Adv Colloid Interf Sci.* 2017;247:100-114.
- 42. Derby B. Inkjet printing of functional and structural materials: fluid property requirements, feature stability, and resolution. *Annu Rev Mater Res.* 2010;40:395-414.
- Liu Y, Derby B. Experimental study of the parameters for stable dropon-demand inkjet performance. Phys Fluids. 2019;31:032004.

- 44. Fromm JE. Numerical calculation of the Fluuid dynamics of drop-on-demand jets. *IBM J Res Dev.* 1984;28:322-333.
- Reis N, Derby B. Ink jet deposition of ceramic suspensions: modelling and experiments of droplet formation. Mater Res Soc Symp Proc. 2000;624:65-70.
- Stow CD, Hadfield MG. An experimental investigation of fluid flow resulting from the impact of a water drop with an unyielding dry surface. Proc R Soc Lond. 1981;373:419-441.
- 47. Derby B. Inkjet printing ceramics: from drops to solid. *J Eur Ceram* Soc. 2011;31:2543-2550.
- 48. Bhola R, Chandra S. Parameters controlling solidification of molten wax droplets falling on a solid surface. *J Mater Sci.* 1999;34:4883-4894.

SUPPORTING INFORMATION

Additional supporting information can be found online in the Supporting Information section at the end of this article.

How to cite this article: Wiegman K, Briot NJ, Hilt JZ, Huckaba AJ, Dziubla TD. Development of branched polyphenolic poly(beta amino esters) to facilitate post-synthesis processing. *J Biomed Mater Res.* 2022;1-13. doi:10.1002/jbm.b.35123